The iron-related molecular toxicity mechanism of synthetic asbestos nanofibres: a model study for high-aspect-ratio nanoparticles

(Article begins on next page)

10 January 2025

UNIVERSITÀ DEGLI STUDI DI TORINO

The iron-related molecular toxicity mechanism of synthetic asbestos nano-fibres: a model study for high aspect ratio nanoparticles.

Francesco Turci,[a] Maura Tomatis,[a] Isidoro G. Lesci,[b] Norberto Roveri,[b] and Bice Fubini*[a]

Abstract: Asbestos shares with carbon nanotubes some morphological and physico-chemical features. An asbestos-like behaviour has been recently reported by some authors, though mechanism of toxicity may be very different. To identify at the atomic level the source of toxicity in asbestos, the effect of progressive iron-loading on a synthetic iron-free model nano-fibre previously found non-toxic in cellular tests was studied. A set of five synthetic chrysotile nano-fibres $[(Mg,Fe)_3(Si_2O_5)(OH)_4]$ has been prepared with Fe ranging from 0 to 1.78 wt. %. The relationship between fibre-induced free-radical generation and the physico-chemical characteristics of iron active sites was investigated with spin-trapping technique on aqueous suspension of the fibres and Mössbauer and EPR spectroscopies on the solids respectively. The fully iron-free fibre was inert, while radical activity arose even with the smallest amount of iron. Surprisingly, such activity decreased upon increasing iron loading. Mössbauer and EPR revealed isolated iron ions in octahedral sites undergoing both axial and rhombic distortion and the occurrence of aggregated iron ions and/or extra-framework clustering. The isolated ions largely prevailed at lowest loadings. Increasing it, the amount of isolated iron was reduced and the aggregation increased. A linear relationship between the formation of carbon-centred radicals and the amount of rhombic-distorted isolated iron sites was found. Even the smallest iron contamination imparts radical reactivity, hence toxicity, to any chrysotile outcrop, discouraging the search for non-toxic chrysotile. The use of model solids only differing in one property at the time appears the most successful approach for a molecular understanding of the physico-chemical determinants of toxicity. Such findings could also be useful in designing safer nano-fibres.

Keywords: asbestos · synthetic chrysotile · iron · EPR · ROS

Introduction

High aspect ratio nanomaterials (HARNs), e.g. carbon nanotubes, nanorods and nanowires,[1] have been found to have an asbestos-like behaviour in animal models.[2] In view of the many promising applications of HARNs, several experimental studies and excellent reviews, in which asbestos are compared to carbon nanotubes (CNTs), have recently appeared.[3] Some animal experiments,[2] but not all,[4] have shown in animal models the development of mesothelioma, a rare type of tumour considered the fingerprint for asbestos exposure,[5] following interaction with CNTs. The discrepancies may be due to differences in the material synthesis, so that the difference between carcinogenic and non carcinogenic HARNs may disclose the key for the design of safer products. HARNs share with asbestos many characteristics which may impart pathogenicity to an insoluble particulate, such as size, shape, presence of transition metal ions and high bio-persistence.[6]

[a] Dr. F. Turci, Dr. M. Tomatis and Prof. B. Fubini
Dipartimento di Chimica I.F.M, NIS Centre of Excellence and Interdepartmental Centre "G. Scansetti" for Studies on Asbestos and Other Toxic Particulates
University of Torino
Via Pietro Giuria, 7 – I-10152 Torino (Italy)
Fax: (+39) 011 6707577
E-mail: bice.fubini@unito.it

[b] Dr. I. G. Lesci, Prof. N. Roveri
Dipartimento di Chimica "G.Ciamician"
University of Bologna
Via Selmi, 2 – I-40126 Bologna (Italy)

((If supporting information is submitted, please include the following line:
Supporting information for this article is available on the WWW under http://www.chemeurj.org/ or from the author.))

In the case of CNTs, the characteristics of the surface[1a;7] and the physico-chemical properties implied in the toxicity mechanisms differ with respect to asbestos. [8] A great attention has been devoted to the role of transition metal ions which may be trapped into framework structure and yield a metal-driven surface reactivity which results in reactive oxygen species (ROS) production.[3;9] In some cases, the simple elimination of metal contaminants remarkably reduces the ROS-derived toxicity effect on cells.[10]

Whether asbestos and HARNs share also common molecular mechanisms of toxicity beside high aspect ratio is presently still a matter of debate. Any attempt to answer this question requires a chemistry-based understanding of the mechanism of toxicity of the considered form of asbestos. Taking into account the complexity of natural asbestos specimens, even within the same mineral species,[11] high purity nanometric, tailored synthetic fibres, which can be modified in one property at the time, need to be considered. Among the various asbestos forms, chrysotile, by far the most used and widespread,[12] is the closed in morphology to many HARNs, including CNTs because of its flexibility and its tangled and curled fibrous form. Thus synthetic chrysotile nanofibres appear the most suitable material to be investigated for a future employment as reference material for HARNs.
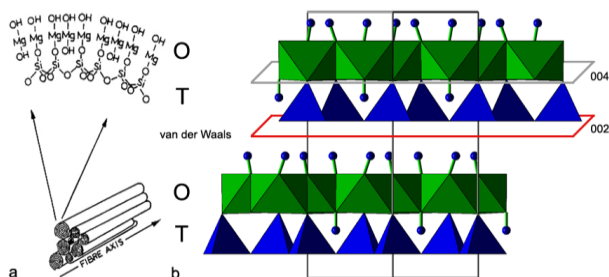
It is widely held that surface reactivity is closely related to the pathological response of asbestos and some other hazardous inhaled particles and fibres.[13] The most robust mechanism-based structure-activity relationship for asbestos includes iron-mediated ROS generation.[14] Iron is absent in the ideal stoichiometric formula of chrysotile $[Mg_6Si_4O_{10}(OH)_8]$, but iron contamination of minerals always takes place in nature. In the case of chrysotile, because of the similarity of charge and size, Fe^{2+} substitutes for Mg^{2+} up to c. 5% in the crystal structure.[15] Chrysotile consists of a tetrahedral silicate sheet arranged in a pseudo-hexagonal network that is joined to an octahedral brucite-like layer formed by edge-sharing octahedral (see Scheme 1). This is the layer where iron can replace magnesium. In

these structures the silicate layer lies on the inside and the brucite layer on the outside of the fibre.

Scheme 1. a) Chrysotile structure adapted from Fubini and Otero, 1999.[14b] b) Crystal structure of chrysotile (XtalDraw[16] adapted from lizardite by Mellini, 1982[17]) as seen along [110]. Silica tetrahedra (T) share an apical oxygen with octahedral brucitic layers (O), while the other three oxygens are electrostatically bound to OH groups from the octahedral layer. The scheme reports the 002 and 004 crystallographic planes.

The present work is the final step of a multidisciplinary study devoted to unveil, at a molecular level, the mechanism of iron-related toxicity by using, for the first time as model solid, a pure and synthetic chrysotile asbestos form. This study has been developed along the following lines:

1. a stoichiometric, geoinspired, iron-free chrysotile nanofibre was synthesized via hydrothermal procedure;[18]
2. the iron-free chrysotile was compared to a natural chrysotile (UICC standard sample). Opposite to natural specimen, no cytotoxic and no oxidative stress nor DNA damage in several *in vitro* tests were reported upon contact with the synthetic iron-free nanofibre;[19]
3. an iron-doped synthetic chrysotile was consequently synthesised with the same synthesis procedure;
4. the iron-doped synthetic chrysotile was shown to be active in ROS production, to induce oxidative stress *in vitro* and to be as toxic as natural UICC chrysotile, providing for the first time, without confounding factors, a direct cause-effect correlation between cellular toxicity and occurrence of iron in asbestos;[20]
5. a set of five Fe-doped synthetic chrysotile fibres, having features consistent with both natural and iron-free synthetic fibres, was synthesised;[21]

Finally, as we report here, the set of fibres have been exploited to clarify the following issues: i) whether extremely low iron loadings (down to 0.67 wt. %) are sufficient to trigger free-radical release thus imparting toxic properties to synthetic nanofibres; ii) the effect of variation in iron-loading on radical release; iii) last but not least, the correlation between position of iron active sites in the crystal lattice and their potential to generate free radicals. Adopting the well-known spin-trapping technique, associated with electron paramagnetic resonance spectroscopy (EPR), we have measured the amount and type of fibre-derived free radical species by contacting chrysotile nano-fibres with hydrogen peroxide and formate ion. Iron sites, responsible for nano-fibres reactivity, have been monitored and characterized by solid-state EPR and ^{57}Fe Mössbauer spectroscopies, with the aim to correlate reactivity relevant to toxicity with peculiar crystallographic feature and lattice distortion of iron sites.

A mechanistic understanding of the nature of iron sites which are relevant for toxicity in asbestos, go well beyond the field of asbestos

toxicity and may be of guidance for future designing of safer HARNs.

Results and Discussion

Qualitative and quantitative measure of free radical generation in a suspension of asbestos fibres

Two biologically relevant reactions, which may yield the formation of radical species, were used to investigate the chemical nature of the exposed iron ions at the surface of asbestos fibres.[13b] In the first mechanism, generally described as a Fenton-like reaction (1.1) occurring at the fibre surface,[22] H_2O_2 reacts with ferrous iron ions:

$$Fe^{2+}_{surf} + H_2O_2 \rightarrow Fe^{3+}_{surf} + OH^- + \bullet OH \qquad (1.1)$$

The release of HO$^\bullet$ radicals in the presence of hydrogen peroxide simulates the reaction that may occur when asbestos fibres, following phagocytosis by alveolar macrophages and recruited polymorphonucleated cells (PMN), are exposed to lysosomal fluids. The reaction may take place also in the presence of Fe^{3+} which is known to be reduced by H_2O_2 to ferrous iron (1.2):[23]

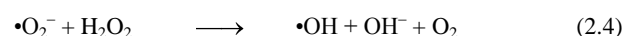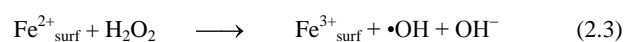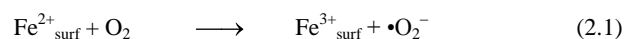$$Fe^{3+}_{surf} + H_2O_2 \longrightarrow Fe^{2+}_{surf} + \bullet O_2^- + 2H^+ \qquad (1.2)$$
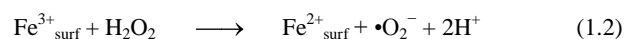
In a normal cellular system, the potential adverse effects of these chemical species are minimized by the antioxidant defences of the cell. However, in the presence of asbestos fibres exposing transition metal ions (markedly iron) the radical species $\bullet O_2^-$, molecular oxygen and H_2O_2 will likely generate the hydroxyl radical ($\bullet OH$). ROS are capable of causing DNA damage,[24] protein oxidation and lipid peroxidation.[14b] When the production of (ROS) and intracellular free radicals overrides the antioxidant capacity of a target cell, oxidative stress arises. Oxidative stress is one of the main epigenetic mechanisms that contributes to all three stages –i.e. initiation, promotion and progression– of carcinogenesis.[25]

The second reaction used to investigate the iron-related reactivity of asbestos is the cleavage of the C–H bond in the formate ion (2) which can be taken as a model reaction that may occur with several molecules of biological interest such as peptides, proteins and lipids. Such reaction yields the formation of a carbon centred radical $CO_2^{-\bullet}$.

$$H - CO_2^- \xrightarrow{Fe^{2+}/Fe^{3+}} \bullet CO_2^- + H^+ + e^- \qquad (2)$$
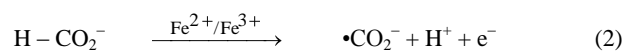
The mechanism is still partially obscure. A direct surface-assisted homolytic cleavage possibly occurs on redox-reactive transition metal, e.g. iron. Alternatively, or even complementarily, molecular oxygen can be reduced to superoxide anion by ferrous iron (Eq. 2.1), initiating a ROS-mediated mechanism sustained by Haber-Weiss cycle.

$$Fe^{2+}_{surf} + O_2 \longrightarrow Fe^{3+}_{surf} + \bullet O_2^- \qquad (2.1)$$

$$2 \bullet O_2^- + 2 H_2O \longrightarrow H_2O_2 + O_2 + 2 OH^- \qquad (2.2)$$

$$Fe^{2+}_{surf} + H_2O_2 \longrightarrow Fe^{3+}_{surf} + \bullet OH + OH^- \qquad (2.3)$$

$$\bullet O_2^- + H_2O_2 \longrightarrow \bullet OH + OH^- + O_2 \qquad (2.4)$$

$$\bullet OH + HCO_2^- \longrightarrow H_2O + \bullet CO_2^- \qquad (2.5)$$

Hydrogen peroxide, yielded via dismutation of the superoxide anion (Eq. 2.2), can react with surface iron via Fenton's reaction (Eq. 2.3) or can further combine with superoxide (Eq. 2.4). Both reactions yield the formation of a highly reactive hydroxyl radical, which in turns can promote the homolytic cleavage of the C–H bond in formate anion (Eq. 2.5). The carboxyl radical is stabilized by resonance and is the unique radical specie which can practically be detected via spin trapping technique under such experimental condition (i.e. relatively high concentration of HCO_2^- and neutral pH). It is note worthy that surface iron involved in this peculiar reactivity has to be accessible and prone to change redox state. The nature of the free-radical generating iron ions is not yet completely clear. It has been reported by many that crocidolite asbestos (one of the most iron-rich asbestos mineral) could be detoxified increasing
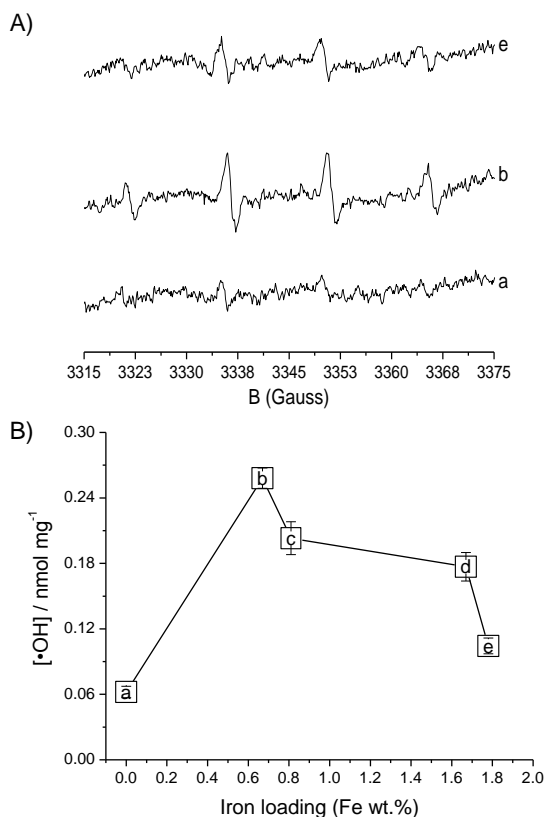
A)

B)

Figure 1. $^{\cdot}$OH radical release from aqueous suspensions of geoinspired chrysotile fibres. Fibres were incubated (10 mg/ml) with hydrogen peroxide solution (0.08 mM, 1 M PB, pH 7.4) in the presence of the spin trapping reagent DMPO. A) Representative EPR spectra of the [DMPO-OH]$^{\cdot}$ adduct of iron-free and iron-loaded chrysotile and B) the area of the integrated EPR signals are reported as function of iron loading (a, 0 %; b, 0.67 %; c, 0.81 %; d, 1.67 %; e, 1.78 %). Data are expressed as mean ± S.E. of at least two independent experiments.

iron amount as the surface, by treating the fibre with ferric iron salts.[26 and ref. therein] On the other hand, tremolite, an amphibole with iron content lower than 5 wt.%,[15] is often compared to crocidolite and amosite –in which Fe content is higher than 20 wt.%– in terms of potency to induce malignant mesothelioma in asbestos miners.[27] Nevertheless, many studies have much increased our knowledge of the physico-chemical features of these aforementioned reactive sites.[11;23;28] For asbestos, the ability of surface iron to generate free radicals appears not related to total iron content, but to the occurrence of some iron surface sites which become active only when present in a specific redox and coordination state.[14c and ref. therein;29] By performing reductive and oxidative treatments on asbestos fibres, it was possible to demonstrate that ferrous iron was

more reactive than ferric iron and by removing (leaching) or adding (impregnating) iron ions that the amount of ferrous ion in a mineral may not be a prerequisite for its activity, hypothesizing that the coordination of ferrous ion to other neighbouring ions may determine its reactivity as well. Using two natural chrysotile specimens, some of us have recently reported that the reactivity of iron ions with unsaturated coordinative valencies was higher than that of ions which are more tightly coordinated to crystal lattice.[11]

In Figure 1A are reported the representative EPR signals recorded after 30 min of contact between the H_2O_2 solution and the synthetic fibres loaded with 0 (a), 0.67 (b) and 1.78 (e) wt.% of Fe^{3+} ions. As previously reported,[20] the iron-free chrysotile does not generates free radicals from the target molecule H_2O_2. On the contrary, the well-known [DMPO-OH]• adduct is detected upon contacting H_2O_2 solution with iron-doped synthetic chrysotile, both at the lowest and the highest iron loading (spectra *b* and *e*,
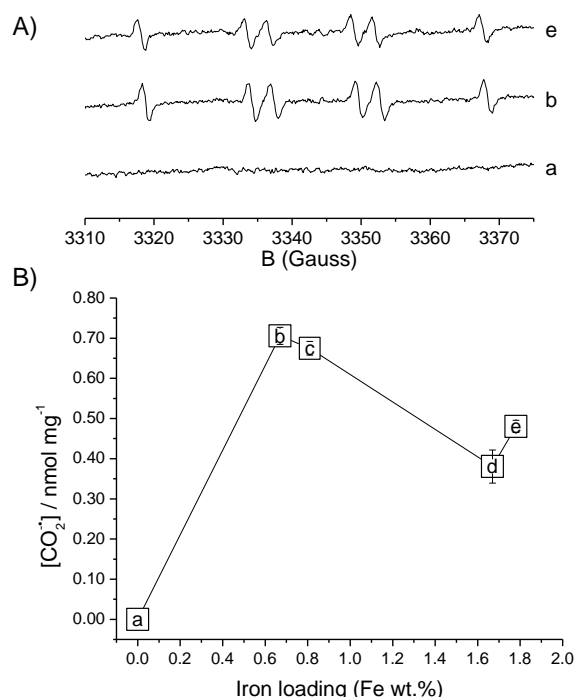
A)

B)

Figure 2. Effect of the presence of ascorbic acid as reducing agent on the iron-induced cleavage of C–H bond by synthetic chrysotile. Fibres were incubated (10 mg/ml) with 2 mM AA solution and 1 M sodium formate solution (1 M PB, pH 7.4) in the presence of the spin-trapping reagent DMPO. A) Representative EPR spectra of the [DMPO-CO$_2^-$]$^{\cdot}$ adduct, recorded after 60 min of incubation, are reported and B) the area of the integrated EPR signals are reported as function of iron loading (a, 0 %; b, 0.67 %; c, 0.81 %; d, 1.67 %; e, 1.78 %). Data are expressed as mean ± S.E. of two independent experiments.

respectively). Since the intensity of the EPR signal is proportional to the concentration of radical species in solution, the signals were integrated and the nmol of radicals produced for unit of chrysotile mass is reported in Figure 1B. Clearly, the lowest iron loading (0.67 wt.%) gives to chrysotile fibres the potency to release •OH radicals upon contacting with H_2O_2. Any further insertion of iron ions in the chrysotile structure determines a linear decrease in the •OH radical yield in solution.

The radical yield in the absence of H_2O_2 is commonly investigated with the formate ion as molecular target.[13b] The EPR spectra recorded after contacting synthetic chrysotile with sodium formate

4

for 60 minutes indicated that neither iron-free nor iron-doped synthetic fibres, at any loading, were able to induce the cleavage of C–H bond in formate anion (data not shown). In order to evaluate the presence at fibre surface of any iron-sites which may easily undergo to reduction and eventually become able to induce C–H rupture, ascorbic acid was added to the buffered reaction mixture containing the formate anion and DMPO. Ascorbic acid, which normally occurs in the lung lining layer –though at a lower concentration than that used in the test–, is only one from several metabolites that can act as reductant in vivo.[30]

In a mild-reducing environment, i.e. 2 mM ascorbic acid, the iron-free chrysotile is still inert in terms of free radical production. Conversely, all other iron-doped samples become active in the C–H cleavage, thus inducing the formation of the carbon-centred $CO_2^{-\bullet}$ radical detected by EPR (Figure 2A). Such finding confirms that only ferrous, and not ferric, iron is involved in the radical reactivity towards C–H bond.[28b] In the panel B, Figure 2, the integrated EPR signals, plotted as nmol of radical per chrysotile mass, are reported. Also using this mechanism of radical production, the lowest amount of iron (0.67 wt.%) generates the highest amount of $CO_2^{-\bullet}$ radicals in solution and the increasing of Fe-doping progressively reduces the reactivity, until a plateau is reached.

The reported decrease in terms of radical reactivity with respect to iron doping may be due to several factors. However, the specific surface area is unchanged with iron content (55 m^2/g and 52 m^2/g for 0 wt.% and 1.78 wt.% of Fe, respectively) and the size and shape of the rolled chrysotile structure is unaltered throughout the series. Since redox properties of surface metals are related to neighbouring atoms,[31] the reduction of radical reactivity could be related to some changes in the coordinative state of trivalent iron, which is know replace both Mg octahedral structural ions and Si tetrahedral ones.[15] Furthermore, the increasing of loading is know to alter transition metals reactivity when groups of aggregated ions are formed.[32] This can occur upon formation of Fe–O–Fe aggregates or nanometric iron oxides within the chrysotile structure.[33]

Iron-specific spectroscopies (Mössbauer and EPR) have been employed to understand the cause of the toxicity-related change in redox reactivity of synthetic asbestos fibres.

^{57}Fe Mössbauer spectroscopy

Mössbauer spectroscopy is unique in its sensitivity to investigate on small variations in the interaction between an active Mössbauer nucleus, such as iron, and its chemical environment. Due to its non-zero nuclear spin, ^{57}Fe is the only Mössbauer-active iron among the four naturally occurring iron isotopes. However, ^{57}Fe low natural abundance (2.1%) requires both long experimental time and large amount of sample. Within our Fe-doped series, only the Mössbauer spectrum of the 1.78 wt.% iron-loaded synthetic chrysotile could be recorded. In Fig. 6, the experimental plot, collected at 11 K, shows a typical absorption, centred at slightly positive velocity values, attributable to the presence of paramagnetic Fe^{3+} species. The best

fitting (black line) was obtained by using two Fe^{3+} components whose parameters, reported in Tab. 1, describe a tetrahedral and an octahedral site, dashed and dotted line respectively.

Figure 6. Mössbauer spectrum of iron-loaded synthetic chrysotile (1.78 %), collected at 11 K.

Though affected by a 5% instrumental error, the relative amount of octahedral and tetrahedral iron was estimated to be 85 and 15 % respectively. The excess of iron in octahedral sites is consistent with chrysotile structure, where Fe predominantly substitutes for hexacoordinated Mg, and with previous spectroscopical reports on this set of samples.[21b] Furthermore, the spectrum suggested that no traces of magnetic species, like iron oxides, even of nanometric size, were present in the sample.

Table 1: Mössbauer parameters: T for tetrahedral, O for octahedral sites

δ (mm/s)	Δ (mm/s)	Γ (mm/s)	A (%)	Attribution
0.21	0.44	0.26	15	Fe^{3+} T
0.35	0.63	0.66	85	Fe^{3+} O

Solid-state EPR investigation of paramagnetic iron

Solid-state EPR spectroscopy is a powerful analytical technique to investigate paramagnetic centres in synthetic and natural minerals, glasses, ligands and protein.[34 and ref. therein] The ferric iron incorporated into the fibre framework during chrysotile synthesis, is paramagnetic in its fundamental electronic state (free ion term = $^6S_{5/2}$). The main spectral features of the EPR spectra of high-spin Fe^{3+} are usually determined by the zero field splitting (ZFS) parameters D and E, which are very sensitive to the environment of the ions, in the present case strength and symmetry of the crystal field.[35] The spin Hamiltonian operator for Fe^{3+}, generally reported at the second order approximation, is:

$$\hat{H} = \mu_B \mathbf{B} \cdot \mathbf{g} \cdot \mathbf{S} + D\left[S_z^2 - \frac{1}{3}S(S+1) \right] + E(S_x^2 - S_y^2) \qquad (1)$$

where μ_B is the Bohr magneton, $\mathbf{S}$ the spin vector with components of spin S_x, S_y, S_z along three mutually perpendicular crystalline axes x, y and z, D and E the usual second-order crystal field terms with axial and rhombic symmetry, and $\mathbf{B}$ the applied magnetic field. The calculation of the spin-Hamiltonian parameters for a high-spin ferric system from experimental data may be more challenging than informative and goes far beyond the purpose of the present paper. An empirical qualitative approach was therefore adopted in interpretation of the EPR data.
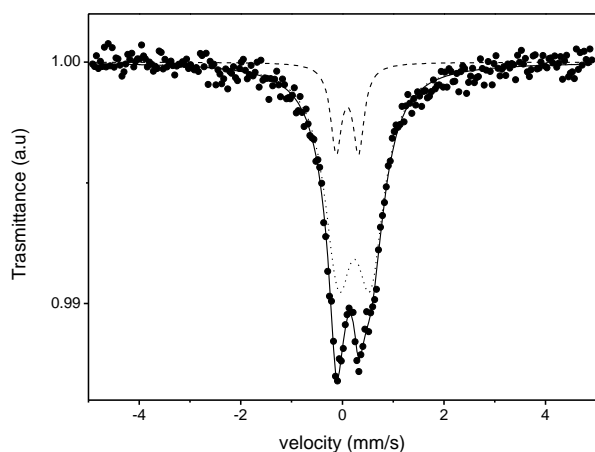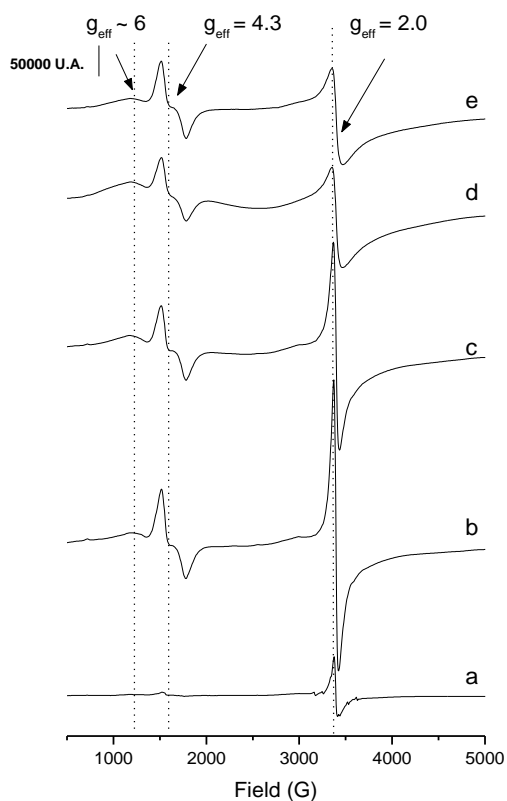
Figure 3. Solid-state EPR investigation of geoinspired synthetic chrysotile. The EPR signal of synthetic chrysotile doped with increasing amounts of iron (a, 0 %; b, 0.67 %; c, 0.81 %; d, 1.67 %; e, 1.78 %) were recorder in vacuum at 77 K. Relative scale bar is reported.

The X-band EPR spectra of synthetic chrysotile were recorded in vacuum at 300 and 77 K and at increasing microwave power, namely 0.1, 1 and 10 mW. The spectra recorded at 77 K were similar to ones recorded at room temperature (data not shown) and, upon increasing power, only the signal to noise ratio increased. Only the dataset recorded at 77 K and 10 mW is hence reported (Fig. 4) for iron-free (a) and iron-doped (b–e) synthetic chrysotile. The iron-free chrysotile spectrum shows only a negligible contribution at g ≈ 2, likely due to some sub-analytical amount Fe^{3+} and Mn^{2+}, the latter recognizable for the six small lines superimposed to the iron signal. All the other spectra from iron-doped fibres are distinctively characterized by two prominent features, which occur at effective g-values (g_{eff})[1] of 2.0 and 4.3, and by a less intense resonance at g_{eff} ≈ 6. A very broad asymmetric resonance at g_{eff} ≈ 2, superimposed to the other sharper features, is observed as iron loading increases (spectra c, d, and e). Line widths (ΔH) of the two main adsorptions at g_{eff}=4.3 and g_{eff}=2.01 were measured from peak to peak: the low-field signal width does not vary upon increasing iron-doping and is always larger than the isotropic component g_{eff}=2.01. At the opposite, a moderate broadening of this latter signal is observed with increasing iron doping.

Several theoretical and experimental studies[36] have confidently assigned the g_{eff} = 4.3 isotropic resonance to isolated octahedral or tetrahedral high-spin Fe^{3+} under rhombic distortion and the resonance at g_{eff} ≈ 6 to axially-distorted ferric ions. The g_{eff} ≈ 6 is usually reported to be coupled with singularity at g ≈ 2, which are observed when ZFS parameter E = 0. Since in the iron-doped synthetic samples investigated in this study Fe is in the chrysotile

---

[1] Effective g-value (g_{eff}) are defined by the resonance condition: $g_{eff} = h\nu_0/\mu_B B$, where B is the resonant field and ν_0 the applied microwave frequency.

octahedral framework, the resonances at g_{eff} = 4.3 and 6 may only arise from O-site Fe^{3+}, which has undergone strong rhombic distortion and axial distortion respectively. A less unambiguous assignment is proposed for the feature at g_{eff} = 2: the intense adsorption could be due to the superimposition of at least two distinct components, one narrow and one broader, both arising from iron ions. The sharper line likely origins from the $|-½\rangle \leftrightarrow |½\rangle$ EPR transition of the high spin Fe^{3+}. A shoulder on both the low- and high-field sides of the g = 2 signal is superimposed, with the low-field signal better resolved while the high-field shoulder is partly buried under the central line. These broader components can be assigned to singularities in the powder patterns of the $|-\frac{5}{2}\rangle \leftrightarrow |-\frac{3}{2}\rangle$, $|-\frac{3}{2}\rangle \leftrightarrow |-\frac{1}{2}\rangle$, $|\frac{1}{2}\rangle \leftrightarrow |\frac{3}{2}\rangle$, and $|\frac{3}{2}\rangle \leftrightarrow |\frac{5}{2}\rangle$ EPR transitions originated from the same single Fe^{3+} site. Alternatively the broad components could arise from another Fe^{3+} ion with a different set of ZFS parameters. Q-band spectra could solve this complex signal, as reported by Goldfarb,[36e] but this would lead the discussion further beyond the purpose of this work. In fact, the most relevant change in the g ~ 2 resonance is the broadening observed upon increasing iron-loading (Fig. 4, spectra b to e). Several reasons could account for this spectral change, i.e. i) overlapping signals from iron in different sites,[37] ii) iron in strong crystal field (low-spin Fe),[36d] iii) iron-clustering with the formation of superexchange multiplet[38] and iv) extraframework iron or separate ferric oxide phases.[36f] The occurrence of iron in framework sites other than octahedral (i) is very small, since Mössbauer data confirms that the substitution of tetrahedral Si with ferric iron is lower than 15% at the highest iron-loading. The occurrence of low-spin iron (ii) is unlikely, since possible octahedral ligands in chrysotile (framework oxygen, hydroxide and eventually water) provide a weak ligand field thus leading to high-spin electronic configuration.[36e] Iron-clustering (iii) and the occurrence of separate iron oxide phases (iv) are both compatible with the observed spectral changes and may account for the loss in term of radical reactivity.[39] Mössbauer spectroscopy indicated that the formation of separate iron oxide phases does not occur. Therefore, the most likely event able to segregate iron, while the overall Fe-loading is increased, is the formation of framework clusters where iron likely partially losses the high redox-reactivity of isolated ion.
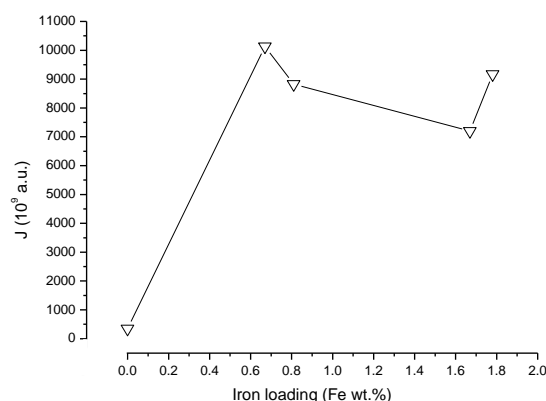
Figure 4. Intensity of the EPR adsorption lines reported as J values ($J=I\cdot(\Delta H)^2$) for the low-field feature at g_{eff}=4.3 recorded at 77K. Data are plotted as function of iron loading.

In order to better investigate the variations in the dispersion of iron ions in the chrysotile framework upon iron loading, we have attempted a rough estimate of the intensities of the various spectral

components. This has been achieved, as usually done, by assuming the intensity of the absorption line J, being $J = I (\Delta H)^2$, where I is the peak-to-peak intensity and ΔH the corresponding line-width of the derivative plot.[40] The iron concentration dependence of J for the low-field adsorption at g_{eff}=4.3, recorded at 77K, is reported in Fig. 4. Since the measurement of the line width for high-field adsorption (g_{eff}=2.01) is quite challenging and can lead to biased results, calculated $J_{g=2}$ values were not reported. The quantification of low-field adsorptions (g_{eff}=4.3) clearly highlights the modification of the EPR signal as a function of iron loading. The $J_{g=4.3}$ value is negligible for iron-free chrysotile and increases dramatically upon doping chrysotile with the lowest amount of iron (Fe wt% = 0.67). Further increase of iron amount (Fe wt% = 0.81 and 1.67) yields an iron loading-dependent decrease of $J_{g=4.3}$ value. At maximum iron loading (Fe wt% = 1.78) the adsorption of g_{eff}=4.3 feature is only slightly lower than J of the sample at the lowest iron loading. The discontinuous trend of the iron-dependent value of $J_{g=4.3}$ could be related to a non-linear process of iron segregation during synthesis, which would yield doped chrysotile including an amount of isolated iron ions unrelated to the actual iron content in the fibre.

To further elucidate what type of iron site are involved in chrysotile reactivity we have compared the variation of the spectral features with the free radical yield. Fig. 5, A and B show the $J_{g=4.3}$ values reported as a function of the radical yield measured upon contacting the synthetic chrysotile samples with HCO_2^- and H_2O_2 respectively. An almost linear dependence of $J_{g=4.3}$ vs. the amount of [$\bullet CO_2^-$] radical is evidenced in figure 5A. A linear regression indicated a correlation of adjusted $R^2 = 0.87$. This clearly suggests that the $\bullet CO_2^-$ free-radical yield is not-only ferrous iron-dependent, but also correlates with isolated iron ions with rhombic distorted crystalline field. Such ions, when exposed at the chrysotile surface, are likely to be the most easily reduced to iron (II) and prone to become reactive in toxicity-related radical production. On the other hand, the mechanism of $\bullet OH$ generation seems to be independent from the lattice distortion which affect hexacoordinated iron in the chrysotile octahedral site. The linear regression estimated from ([$\bullet OH$], J) plot gives in fact an adjusted R^2 of 0.41 which confirms the uncorrelation of the two variables.
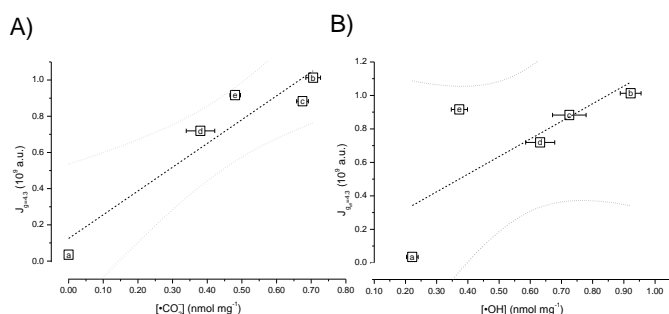
Experiments on one set of model fibres, iron-free vs. iron-doped, has confirmed the role of iron in this toxicity-relevant asbestos reactivity, clarifying at atomic level the nature of surface site responsible for ROS generation.

We have observed that a fibre which does not expose iron is non-reactive in terms of ROS generation and cellular damage. However, on the basis of the present and past studies, we have clear evidence that even a very small amount of iron induces radical reactivity, cytotoxcity and genotoxicity. Any further increase in iron-loading progressively decreases, instead of increasing, the reactivity. The hypothesised catalytic role of iron in asbestos-related ROS production, for a long time only indirectly reported by chemists and toxicologists, is here directly confirmed. In particular, the potential to generate carbon-centred radicals is here clearly assigned to iron ions with rhombic distorted crystalline field, more likely to be reduced and participate in redox-reactive cycles.

Our results do not support the existence in nature of any non-toxic chrysotile form. In fact, it is well know that any mineral, including chrysotile, iron contamination ineluctably takes place. It is therefore definitely unlikely that chrysotile fibres fully deprived of iron, thus possibly non toxic, might be found. Moreover, due to the tendency of Mg to be replaced by Fe, iron may be acquired from many sources during extraction and processing or even *in vivo*.

In conclusion the employment of model solids only differing in one property is the clue for the understanding the mechanisms of particle and fibre toxicity at the molecular/surface site level. On such basis, any effort in the design of safer micro- and nano-materials and particularly HARNs should proceed by modifying step by step the physico-chemical properties know to be related to health effects.

Experimental Section

Synthetic chrysotile asbestos: A hydrothermal synthesis reactor (Parr Stirred "Mini" reactor model 4652) with a 500cm^3 moveable vessel constructed with "alloy C-276" (a metal alloy containing 6.5% wt Fe), was used to carry out the hydrothermal reaction of SiO_2 – Aerosil 380 as a powder with a surface area of about 380m^2/g (Eigenmann & Veronelli S.p.A.) – and $MgCl_2$ in an aqueous NaOH solution up to pH 13 and at temperature of 300 °C on the saturated vapour pressure curve (82 atm) with a run duration of 24 h. The precipitate removed from the solution was repeatedly washed with deionized water before being dried for 3 h at 150 °C. To synthesise the series of Fe-doped chrysotile samples, a gel mixture of SiO_2, $FeCl_3$ and $MgCl_2$ in an aqueous solution was prepared. The pH of the gel mixture, containing a Si/(Mg + Fe) molar ratio in the interval 0.6–0.7, was adjusted to 13 by means of an aqueous NaOH solution. We have used concentrations of $MgCl_2$ and $FeCl_3$ ranging from 9.75 up to 10mM. The precipitate removed from the solution was repeatedly washed with deionized water before being dried for 3 h at 150 °C.

Reagents: 5,5-Dimethyl-1-pyrroline-N-oxide (DMPO) was purchased form Alexis (Lausen, Switzerland); the other reagents were purchased from Sigma-Aldrich (St. Louis, MO – USA). In all experiments ultrapure MilliQ (Millipore, Billerica, MA – USA) water was used.

Surface-area measurements: The surface area was measured by means of BET methods based on N2 adsorption at 77 K (Micrometrics ASAP 2020)

Generation of free radicals: In order to detect the formation of radicals in aqueous suspension of the fibres contacted with H_2O_2 or HCO_2^-, the spin trapping agent DMPO was used. Following a well established technique described in previous studies,[21] the nature and quantity of the stabilized radical was measured by means of Electron Paramagnetic Resonance (EPR) spectroscopy. *Reaction with H_2O_2*: Fibers were suspended (22 mg ml^{-1}) in 0.250 ml of H_2O_2 (0.5 M in H_2O), 0.250 ml of DMPO (0.05 M) and 0.500 ml of potassium phosphate buffer (KPB, 1 M, pH 7.4). *Reaction with HCO_2^-*: Fibers were suspended (22 mg ml^{-1}) in 0.500 ml of HCO_2^- (2 M in KPB 1 M, pH 7.4) and 0.500 ml of DMPO (0.05 M). The radical formation was evaluated by recording at 10, 30, 60 min the EPR spectrum of the adduct. All spectra were recorded on a Miniscope MS 100 (Magnettech, Berlin, Germany) EPR spectrometer. The instrument settings were as follows: microwave power, 10 mW; modulation, 1000 mG; scan range, 120 G; centre of field, c. 3345 G. The number of radicals released is proportional to the intensity of the EPR signal. The signals were double integrated and spin number was

Figure 5. Free radical generation dependency of the g_{eff}=4.3 EPR intensity. J value is reported as function of [$\bullet CO_2^-$] (A) and [$\bullet OH$] (B) free radical yield, expressed as nmol of radicals per mass unit of synthetic chrysotile, measured via spin-trapping technique (see Figs 1 and 2). Letters indicate the iron loading for each chrysotile sample (a, 0 %; b, 0.67 %; c, 0.81 %; d, 1.67 %; e, 1.78 %). Linear fit and confidence bands (95%) for each experimental dataset are reported.

Conclusion

reported, as nmol per unit mass of chrysotile. Blanks were performed in parallel in the absence of any fibre. All the experiments were repeated at least twice.

Solid state EPR spectroscopy: Synthetic chrysotile samples (20 mg) were degassed in a quartz cell at RT. Resonance (EPR) spectra were run using an X-band CW-EPR Bruker EMX spectrometer equipped with a cylindrical cavity operating at 100 kHz field modulation. The measurements were carried out in cells that can be connected to a conventional high-vacuum apparatus (residual pressure $<10^{-6}$ kPa). The spectra were also recorded at liquid nitrogen temperature (77 K). Instrumental settings of spectra reported: microwave power 10 mW, modulation amplitude 5 G, sweep time 350 s, time constant 82 ms, 1 scan.

^{57}Fe Mössbauer spectroscopy: Mössbauer spectroscopy was performed using a conventional constant-acceleration spectrometer with transmission geometry (TMS), using a room temperature Rh matrix ^{57}Co source (nominal strength 1850 mBq). In order to improve the spectrum quality the experiment was performed at 11K by using an ARS® closed circuit cryostat. The hyperfine parameters isomer shift (δ), quadrupole splitting (Δ) and full linewidth at half maximum (Γ), expressed in mm/s, were obtained by means of a standard least-squares minimisation technique. The spectrum was fitted to Lorentzian line shapes using the minimum number of doublets. The isomer shift was relative to metallic iron at room temperature.

Acknowledgements

Reference List

[1.]   Tran, C. L., Hankin, S. M., Ross, B., Aitken, R. J., Jones, A. D., Donaldson, K., Stone, V., and Tantra, R. An outline scoping study to determine whether high aspect ratio nanoparticles (HARN) should raise the same concerns as do asbestos fibres. Report on Project CD0406 [http://www.safenano.org/Uploads/HARN.pdf]. 13-8-2008. Edinburgh, UK, Institute for Occupational Medicine.

[2.]   a) C. A. Poland, R. Duffin, I. Kinloch, A. Maynard, W. A. H. Wallace, A. Seaton, V. Stone, S. Brown, W. MacNee, K. Donaldson, Nature Nanotechnology 2008, 3 423-428. b) A. Takagi, A. Hirose, T. Nishimura, N. Fukumori, A. Ogata, N. Ohashi, S. Kitajima, J. Kanno, The Journal of Toxicological Sciences 2008, 33 105-116.

[3.]   a) K. Kostarelos, Nat.Biotechnol. 2008, 26 774-776. b) M. C. Jaurand, A. Renier, J. Daubriac, Part Fibre.Toxicol. 2009, 6 16. c) A. B. Kane, R. H. Hurt, Nat.Nanotechnol. 2008, 3 378-379. d) A. A. Shvedova, E. R. Kisin, D. Porter, P. Schulte, V. E. Kagan, B. Fadeel, V. Castranova, Pharmacology & Therapeutics 2009, 121 192-204. e) V. C. Sanchez, J. R. Pietruska, N. R. Miselis, R. H. Hurt, A. B. Kane, Nanomed.Nanobiotechnol. 2009, 511-529.

[4.]   J. Muller, M. Delos, N. Panin, V. Rabolli, F. Huaux, D. Lison, Toxicological Sciences 2009, 110 442-448.

[5.]   J. C. Wagner, C. A. Sleggs, P. Marchand, Br J Ind Med 1960, 17 260-271.

[6.]   P. Borm, V. Castranova, Particle and Fibre Toxicology 2009, 6 .

[7.]   a) B. Fubini, I. Fenoglio, M. Tomatis, in Nanotoxicology: characterization, dosing and health effects, Informa Healthcare, New York 2005, p. pp. 59-70. b) I. Fenoglio, M. Tomatis, D. Lison, J. Muller, A. Fonseca, J. B. Nagy, B. Fubini, Free Radic.Biol.Med. 2006, 40 1227-1233.

[8.]   a) I. Fenoglio, G. Greco, M. Tornatis, J. Muller, E. Rayrnundo-Pinero, F. Beguin, A. Fonseca, J. B. Nagy, D. Lison, B. Fubini, Chem.Res.Toxicol. 2008, 21 1690-1697. b) J. Muller, F. Huaux, A. Fonseca, J. B. Nagy, N. Moreau, M. Delos, E. Raymundo-Pinero, F. Beguin, M. Kirsch-Volders, I. Fenoglio, B. Fubini, D. Lison, Chem.Res.Toxicol. 2008, 21 1698-1705.

[9.]   A. E. Nel, L. Madler, D. Velegol, T. Xia, E. M. V. Hoek, P. Somasundaran, F. Klaessig, V. Castranova, M. Thompson, Nature Materials 2009, 8 543-557.

[10.]   K. Pulskamp, S. Diabate, H. F. Krug, Toxicology Letters 2007, 168 58-74.

[11.]   F. Turci, S. E. Favero-Longo, M. Tomatis, G. Martra, D. Castelli, R. Piervittori, B. Fubini, Chemistry 2007, 13 4081-4093.

[12.]   G. Tweedale, Nat.Rev.Cancer 2002, 2 311-315.

[13.]   a) M. F. Hochella, in Health Effects of Mineral Dust - Reviews in Mineralogy ,Vol. 28, (Eds.: G. D. Jr. Guthrie, B. T. Mossman), The Mineralogical Society of America, Washington, DC - USA 1993, p. pp. 275-308. b) B. Fubini, L. Mollo, E. Giamello, Free Radic.Res. 1995, 23 593-614. c) B. Fubini, Environ.Health Persp. 1997, 105 Suppl 5 1013-1020. d) D. Hohr, Y. Steinfartz, R. P. Schins, A. M. Knaapen, G. Martra, B. Fubini, P. J. Borm, Int.J.Hyg.Environ.Health 2002, 205 239-244.

[14.]   a) IARC, Monograph on the evaluation of the carcinogenic risk of chemicals to humans: A review of human carcinogens, 2010. b) B. Fubini, C. Otero-Areán, Chem.Soc.Rev. 1999, 28 373-381. c) A. Shukla, M. Gulumian, T. K. Hei, D. W. Kamp, Q. Rahman, B. T. Mossman, Free Radic.Biol.Med. 2003, 34 1117-1129.

[15.]   W. A. Deer, R. A. Howie, J. Zussman, An introduction to the rock-forming minerals., 2nd ed. Longman, London, UK 1992.

[16.]   Downs, R. T., Bartelmehs, K., and Sinnaswamy, K. Computer code XtalDraw, a program for drawing crystal structures. 2003. Tucson, AZ, University of Arizona. Ref Type: Computer Program

[17.]   M. Mellini, Amer.Mineral. 1982, 67 587-598.

[18.]   a) G. Falini, E. Foresti, M. Gazzano, A. E. Gualtieri, M. Leoni, I. G. Lesci, N. Roveri, Chemistry 2004, 10 3043-3049. b) G. Falini, E. Foresti, G. Lesci, N. Roveri, Chem.Commun. 2002, 1512-1513.

[19.]   E. Gazzano, E. Foresti, I. G. Lesci, M. Tomatis, C. Riganti, B. Fubini, N. Roveri, D. Ghigo, Toxicol.Appl.Pharmacol. 2005, 206 356-364.

[20.]   E. Gazzano, F. Turci, E. Foresti, M. G. Putzu, E. Aldieri, F. Silvagno, I. G. Lesci, M. Tomatis, C. Riganti, C. Romano, B. Fubini, N. Roveri, D. Ghigo, Chem.Res.Toxicol. 2007, 20 380-387.

[21.]   a) E. Foresti, M. F. Hochella, H. Kornishi, I. G. Lesci, A. S. Madden, N. Roveri, H. F. Xu, Advanced Functional Materials 2005, 15 1009-1016. b) E. Foresti, E. Fornero, I. G. Lesci, C. Rinaudo, T. Zuccheri, N. Roveri, Journal of Hazardous Materials 2009, 167 1070-1079.

[22.]   I. Fenoglio, L. Prandi, M. Tomatis, B. Fubini, Redox.Rep. 2001, 6 235-241.

[23.]   M. Tomatis, L. Prandi, S. Bodoardo, B. Fubini, Langmuir 2002, 18 4345-4350.

[24.]   a) L. G. Lund, A. E. Aust, Carcinogenesis 1992, 13 637-642. b) J. A. Hardy, A. E. Aust, Carcinogenesis 1995, 16 319-325. c) C. Riganti, E. Aldieri, L. Bergandi, I. Fenoglio, C. Costamagna, B. Fubini, A. Bosia, D. Ghigo, Free Radic.Biol.Med. 2002, 32 938-949.

[25.]   a) Y.-T. Woo, D. Y. Lai, in Quantitative Structure-Activity Relationship (QSAR) Models of Mutagens and CarcinogensEd.: R. Benigni), CRC Press, Boca Raton, FL - USA 2003, p. pp. 41-80. b) A. B. Kane, in Mechanisms of fibre carcinogenesisEds.: A. B. Kane, P. Boffetta, R. Saracci, J. D. Wilbourn), IARC - WHO, Lyon, France 1996, p. pp. 11-34.

[26.]   M. Gulumian, J.Toxicol.Environ.Health B Crit Rev. 2005, 8 453-483.

[27.]   Y. Suzuki, S. R. Yuen, Asbestos fibers contributing to the induction of human malignant mesothelioma, 2002, pp. 160-176.

[28.]   a) G. Martra, E. Chiardola, S. Coluccia, L. Marchese, M. Tomatis, B. Fubini, Langmuir 1999, 15 5742-5752. b) G. Martra, M. Tomatis, I. Fenoglio, S. Coluccia, B. Fubini, Chem.Res.Toxicol. 2003, 16 328-335.

[29.]   D. Bernstein, V. Castranova, K. Donaldson, B. Fubini, J. Hadley, T. Hesterberg, A. B. Kane, D. Lai, E. E. McConnell, G. Muhle, G. Oberdorster, S. Olin, D. B. Warheit, Inhalation Toxicology 2005, 17 497-537.

[30.]   M. H. Bui, A. Sauty, F. Collet, P. Leuenberger, J.Nutr. 1992, 122 312-316.

[31.]   a) A. Zecchina, G. Spoto, G. Ghiotti, E. Garrone, Journal of Molecular Catalysis 1994, 86 423-446. b) B. Fubini, V. Bolis, A. Cavenago, E. Garrone, P. Ugliengo, Langmuir 1993, 9 2712-2720.

[32.]   a) G. Berlier, F. Bonino, A. Zecchina, S. Bordiga, C. Lamberti, Chemphyschem 2003, 4 1073-1078. b) A. V. Kucherov, C. P. Hubbard, M. Shelef, Journal of Catalysis 1995, 157 603-610.

[33.]   A. V. Kucherov, M. Shelef, Journal of Catalysis 2000, 195 106-112.

[34.]   B. Sutter, T. Wasowicz, T. Howard, L. R. Hossner, D. W. Ming, Soil Sci.Soc.Am.J. 2002, 66 1359-1366.

[35.]   F. E. Mabbs, D. Collinson, in EPR of Transition metal compounds ,Vol. 16, (Elsevier, Amsterdam 1992, p. pp. 319-337.

[36.]   a) X. Carrier, P. Lukinskas, S. Kuba, L. Stievano, F. E. Wagner, M. Che, H. Knozinger, Chemphyschem 2004, 5 1191-1199. b) S. Bordiga, R. Buzzoni, F. Geobaldo, C. Lamberti, E. Giamello, A. Zecchina, G. Leofanti, G. Petrini, G. Tozzola, G. Vlaic, Journal of Catalysis 1996, 158 486-501. c) A. Parmaliana, F. Arena, F. Frusteri, A. Martinez-Arias, M. L. Granados, J. L. G. Fierro, Applied Catalysis A-

General 2002, 226 163-174. d) J. Castner, G. S. Newell, W. C. Holton, C. P. Slichter, The Journal of Chemical Physics 1960, 32 668-673. e) D. Goldfarb, M. Bernardo, K. G. Strohmaier, D. E. W. Vaughan, H. Thomann, Journal of the American Chemical Society 1994, 116 6344-6353. f) D. Arieli, D. E. W. Vaughan, K. G. Strohmaier, H. Thomann, M. Bernardo, D. Goldfarb, Magnetic Resonance in Chemistry 1999, 37 S43-S54.

[37.] G. Catana, J. Pelgrims, R. A. Schoonheydt, Zeolites 1995, 15 475-480.

[38.] A. F. Reid, H. K. Perkins, M. J. Sienko, Inorganic Chemistry 1968, 7 119-126.

[39.] a) B. Fubini, L. Mollo, Toxicol.Lett. 1995, 82-83 951-960. b) H. L. Karlsson, J. Gustafsson, P. Cronholm, L. Moller, Toxicology Letters 2009, 188 112-118.

[40.] a) R. K. Singh, G. P. Kothiyal, A. Srinivasan, Journal of Non-Crystalline Solids 2008, 354 3166-3170. b) R. K. Singh, G. P. Kothiyal, A. Srinivasan, Solid State Communications 2008, 146 25-29.

Synthetic asbestos: a model for nanofibres molecular toxicity

Francesco Turci, Maura Tomatis, Isidoro G. Lesci, Norberto Roveri, and Bice Fubini*

Iron-related molecular toxicity mechanism of synthetic asbestos nano-fibres: a model study for high aspect ratio nanoparticles

((Insert TOC Graphic here))

((Text for Table of Contents))